Subcell FDTD Modeling of Electrically Thin Dispersive Layers

Mikko K. Kärkkäinen

***Abstract*—A novel technique for treating electrically thin dispersive layers with the finite-difference time-domain (FDTD) method is introduced. The proposed model is based on the subcell technique, where the constitutive relations are locally averaged in the FDTD grid. The most significant feature of the proposed model is its ability to model rather complicated dispersive layers having multiple pole pairs. The model is validated with several numerical examples making comparison with the exact results. Both time- and frequency-domain validations are presented.**

***Index Terms*—Dispersive layers, electrically thin layers, finite difference time domain (FDTD).**

I. Introduction

MANY microwave devices contain electrically thin layers. Therefore, the numerical modeling of such structures is of interest. The finite-difference time-domain (FDTD) method has been widely accepted as an efficient tool for the accurate solving of a great variety of electromagnetic problems. The present problem, modeling of electrically thin dispersive layers, may be solved basically in the following three ways:

1) with direct and fine enough discretization of the fields inside the layer;
2) using the surface impedance boundary conditions (SIBCs);
3) by locally modifying the update equations to account for the layer.

The direct discretization cannot be classified as an efficient method because it may require very dense mesh inside the layer, and unless a nonuniform mesh is used in the FDTD lattice, it results in a dramatic increase of the computational burden. The surface impedance approach is very efficient, but extremely complicated when modeling dispersive layers. The surface impedance method has been usually employed when modeling perfect electric conductor (PEC) backed dielectric and conductive coatings [1]–[3]. The application of the SIBC approach for more general dispersive layers, where the metal backing is not present, leads to transition conditions, which are also very complicated to implement into the FDTD method without making approximations. Penney *et al.* have used the SIBC technique for coated targets by expressing the frequency-domain surface impedance function as a sum of basis functions in [4]. The approximation is rather coarse unless many basis functions are used. A separate routine for finding the optimal coefficients for the basis functions is also needed. The first order Leontovich SIBC was used in [4].

The subcell technique is clearly also an efficient approach since a coarse mesh may be used, and the memory requirements remain almost unchanged after the insertion of the layer provided that the layer fills only a small amount of the computation space. Some models for dielectric and conductive layers based on subcell techniques can be found in the literature. Tirkas and Demarest proposed a model for thin dielectric layers in [5]. Maloney and Smith took a slightly different approach in [6] when modeling dielectric and conductive layers. Some other models have also been suggested [7]–[9], but they have been verified by Maloney and Smith in [10] to be less accurate than the models by Maloney and Smith and Tirkas and Demarest. A disadvantage of the subcell method is its inability to model electrically thick layers. In such situations, one should resort to SIBCs or to direct discretization methods. A direct discretization algorithm has been presented by Young in [11]. Notice that the previous subcell techniques [5]–[9] are not applicable to dispersive layers.

In this paper, we formulate a new subcell technique, which allows modeling quite general dispersive layers, possibly having multiple pole pairs. The proposed model reduces to the model by Maloney and Smith in the case of dielectric and conductive layers. The new model is formulated in the general three-dimensional (3-D) case in Section II, and validation studies are conducted with one-dimensional (1-D) and two-dimensional (2-D) FDTD programs in Section III both in time and frequency domains. Quite good agreement with the analytical results is observed.

II. Subcell Technique for Dispersive Layers

The basic idea of the model is quite simple: we will average the electric and magnetic flux densities so that they will simulate the presence of a thin dispersive layer. The layer is assumed to be located in free space, although this need not necessarily be the case. The field components both tangential and normal to the layer will be affected by the model. Consider deriving the update equations for the tangential magnetic-field components in the vicinity of a dispersive layer of thickness d and with the frequency-dependent isotropic permeability

$$\mu(\omega) = \mu_0 \left(\mu_\infty + \sum_{k=1}^{P} \frac{\beta_{m,k}}{\omega_{0m,k}^2 - \gamma_{m,k}\omega^2 + j\delta_{m,k}\omega} \right) \quad (1)$$

where P is the number of pole pairs and the subscript k refers to the kth pole pair. The subscript m refers to the magnetic layer. An appropriate choice of the parameters in the above expression

Manuscript received November 4, 2002; revised January 13, 2003.

The author is with the Radio Laboratory, Helsinki University of Technology, Helsinki FIN-02015 HUT, Finland (e-mail: mkk@cc.hut.fi).

Digital Object Identifier 10.1109/TMTT.2003.812584

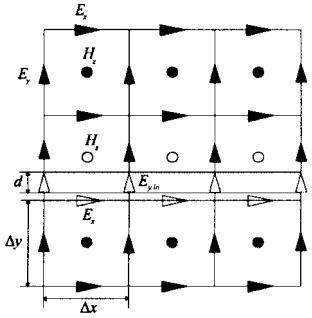

(a)

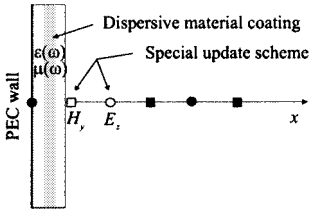

(b)

Fig. 1. (a) Slice of the FDTD lattice in the xy-plane. A special update scheme is developed for the field components denoted with nonfilled objects. Extra variables are introduced for the field components normal to and inside the layer. (b) Problem geometry in a 1-D problem. The reflection of a z-polarized pulse from a coated ideal conductor is studied.

allows us to obtain a layer of Lorentz, Debye, or Drude type as special cases. Similarly, the expression for the permittivity is taken to be of the form

$$\epsilon(\omega) = \epsilon_0 \left(\epsilon_\infty + \sum_{k=1}^{P} \frac{\beta_{e,k}}{\omega_{0e,k}^2 - \gamma_{e,k}\omega^2 + j\delta_{e,k}\omega} \right) \tag{2}$$

with analogous definitions of the parameters as above. Let the layer partially fill a single plane of FDTD cells in the 3-D FDTD lattice. A slice of the FDTD lattice in xy-plane is shown in Fig. 1(a). The geometry of a 1-D interface problem, which is considered later, is shown in Fig. 1(b). If the volume fraction occupied by the layer is α, then we may calculate the averaged magnetic flux density inside the cells containing the dispersive layer according to $\mathbf{B} = \alpha\mu(\omega)\mathbf{H}_{\text{layer}} + (1-\alpha)\mu_0\mathbf{H}_{\text{free space}}$ with $0 \le \alpha \le 1$. Using the magnetic susceptibility $\chi_{m,k}(\omega)$ associated with the kth pole pair, defined as

$$\chi_{m,k}(\omega) = \frac{\beta_{m,k}}{\omega_{0m,k}^2 - \gamma_{m,k}\omega^2 + j\delta_{m,k}\omega} \tag{3}$$

we obtain the equation

$$\mathbf{B} = \alpha\mu_0 \left[\mu_\infty + \sum_{k=1}^{P} \chi_{m,k}(\omega) \right] \mathbf{H} + (1-\alpha)\mu_0\mathbf{H}. \tag{4}$$

As an example, let us derive the update equation for the z-component of the tangential magnetic field [see Fig. 1(a)]. The magnetization $M_{z,k}$ and magnetic field H_z are related through the magnetic susceptibility according to

$$M_{z,k} = \mu_0\chi_{m,k}(\omega)H_z \tag{5}$$

and the magnetic current $K_{z,k}$ may be expressed with the magnetization $M_{z,k}$ as

$$K_{z,k} = j\omega M_{z,k}. \tag{6}$$

From the z-component of the Faraday's law, we obtain the equation

$$\big[1+\alpha(\mu_\infty - 1)\big]\mu_0 \frac{\partial H_z}{\partial t} = -\mathbf{u}_z \cdot (\nabla \times \mathbf{E}) - \alpha \sum_{k=1}^{P} K_{z,k}. \tag{7}$$

The dot product of the curl and the unit vector $\mathbf{u}_z$ picks the z-component from the curl. The discrete form of (7) reads

$$\begin{aligned} H_z|^{n+1/2}_{i,j+1/2,k+1/2} &= H_z|^{n-1/2}_{i,j+1/2,k+1/2} \\ &\quad - \frac{\Delta t}{\big[1+\alpha(\mu_\infty-1)\big]\mu_0} (\nabla \times \mathbf{E})_z|^n_{i,j+1/2,k+1/2} \\ &\quad - \frac{\alpha\Delta t}{\big[1+\alpha(\mu_\infty-1)\big]\mu_0} \sum_{k=1}^{P} K_{z,k}|^n_{i,j+1/2,k+1/2}. \end{aligned} \tag{8}$$

Using the definitions for the magnetization $M_{z,k}$ in (5) and for the magnetic current $K_{z,k}$ in (6), we obtain the auxiliary equation

$$\omega_{0m,k}^2 M_{z,k} + j\omega\gamma_{m,k}K_{z,k} + \delta_{m,k}K_{z,k} = \mu_0\beta_{m,k}H_z. \tag{9}$$

The update equations for the auxiliary variables $K_{z,k}$ and $M_{z,k}$ for any k can now be obtained by discretizing (9) and (6) as follows:

$$\begin{aligned} K_{z,k}|^{n+1}_{i,j+1/2,k+1/2} =& \frac{2\gamma_{m,k} - \delta_{m,k}\Delta t}{2\gamma_{m,k} + \delta_{m,k}\Delta t} K_{z,k}|^n_{i,j+1/2,k+1/2} \\ &+ \frac{2\mu_0\beta_{m,k}\Delta t}{2\gamma_{m,k} + \delta_{m,k}\Delta t} H_z|^{n+1/2}_{i,j+1/2,k+1/2} \\ &- \frac{2\omega_{0m,k}^2\Delta t}{2\gamma_{m,k} + \delta_{m,k}\Delta t} M_{z,k}|^{n+1/2}_{i,j+1/2,k+1/2} \\ M_{z,k}|^{n+3/2}_{i,j+1/2,k+1/2} =& M_{z,k}|^{n+1/2}_{i,j+1/2,k+1/2} \\ &+ \Delta t K_{z,k}|^{n+1}_{i,j+1/2,k+1/2}. \end{aligned} \tag{10}$$

Notice that in the limit $\alpha \longrightarrow 0$ with $\mu_\infty = 1$, the coupling between H_z and auxiliary variables $K_{z,k}$ and $M_{z,k}$ disappears, and we obtain the usual update equation for the magnetic field H_z in free space, as required for consistency of the model. Also, if $\beta_{m,k} = 0$ for all k and $\mu_\infty = 1$, implying that the auxiliary variables are zero, leads to the usual update equations in free space.

The quantity $1 + \alpha(\mu_\infty - 1)$ can be regarded as an averaged relative permeability in the limit $\omega \longrightarrow \infty$. To get the update equation for the normal component of the magnetic field H_y, which is inside the layer, we need to replace $1 + \alpha(\mu_\infty - 1)$ with μ_∞ and set $\alpha = 1$ in (8) and (10) with appropriate changes in the subscripts.

The derivation of the update equations for the electric-field components in the case of a layer in free space is quite analogous and is not shown here. However, in the case when metal is

coated with the layer, we must account for the fact that the tangential electric field decays to zero in the vicinity of the ideal conductor. This situation is most conveniently described in a 1-D case. Suppose that there is an ideally conducting wall at $x = 0$ [see Fig. 1(b)] and let the coating on the wall have a thickness d. Let the electric field be polarized along the z-axis. The PEC wall implies that we have $E_z|_0 = 0$ all the time. The tangential magnetic field at a half-cell away from the PEC wall can be updated as described above. However, the simple averaging of the electric flux density D_z in the vicinity of the PEC wall is not a good approach.

To demonstrate how the PEC wall is accounted for, consider deriving the update equation for the field component $E_z|_1$ in the immediate vicinity of the coating. Usually, the fields are assumed to be piecewise linear across each FDTD cell. Hence, we make a very natural assumption that the electric field behaves linearly in the range $\Delta x/2 < x < 3\Delta x/2$ with the slope chosen so that a linear extrapolation to $x = 0$ would yield a zero electric field. Thus, we assume that

$$E_z(x) = \frac{x}{\Delta x} E_z|_1. \tag{11}$$

Next, we calculate the spatially averaged electric flux density near the wall and use it to deduce the effective permittivity of the coating in the limit $\omega \longrightarrow \infty$. Integrating from $x = \Delta x/2$ to $x = 3\Delta x/2$, we obtain

$$\begin{aligned} D_z|_1 =& \frac{1}{\Delta x} \int_{\Delta x/2}^{3\Delta x/2} \epsilon_{\omega\to\infty}(x) \frac{x}{\Delta x} E_z|_1 \, dx \\ =& \epsilon_0 \left[\frac{9-\epsilon_\infty}{8} + \frac{d^2}{2\Delta x^2}(\epsilon_\infty - 1) \right] E_z|_1 \\ =& \epsilon_0 \epsilon_{r,\infty,\text{ave}}(d, \epsilon_\infty) E_z|_1. \end{aligned} \tag{12}$$

This relation is utilized when updating the electric field near the boundary. The consistency requirements are easy to check. If $\epsilon_\infty = 1$, we have $\epsilon_{r,\infty,\text{ave}} = 1$ regardless of the layer thickness d and if $d = 0$, we obtain $\epsilon_{r,\infty,\text{ave}} = 1$ for $\epsilon_\infty = 1$. Notice that the above derivation is only necessary if the layer thickness $d > \Delta x/2$. For smaller thicknesses, magnetic properties of the layer are known to dominate the shape of the reflected waveform. This fact can be easily seen from the Leontovich SIBC, which takes the form

$$E_z = j\omega\mu(\omega) d H_y \tag{13}$$

if the tangent function in the impedance $Z_s(\omega) = j\eta \tan(kd)$ is approximated with its argument $\tan(kd) \approx kd$. Hence, we may use $\epsilon_{r,\infty,\text{ave}} = 1$ if $d < \Delta x/2$ and the wavelength inside the layer is not very small. In the following section, we will demonstrate a pulse reflection from a wall coated with a layer having a rather complicated frequency dependence of the material parameters.

It was observed from numerical experiments that the conductivity of the layer may be approximated by simple averaging according to $\sigma_{\text{ave}} = \alpha\sigma$, where α is the volume fraction of the layer occupying the adjacent cells to $E_z|_1$. Thus, for a coating of thickness d and conductivity σ, we obtain

$$\sigma_{\text{ave}} = \frac{d}{2\Delta x}\sigma. \tag{14}$$

Introducing the electric polarization current $\mathbf{J}$ and polarization $\mathbf{P}$, we obtain the update equation for the electric field $E_z|_1$ next to the metal wall in the 1-D case

$$\begin{aligned} E_z|_1^{n+1} =& \frac{2\epsilon_{r,\infty,\text{ave}}\epsilon_0 - \sigma_{\text{ave}}\Delta t}{2\epsilon_{r,\infty,\text{ave}}\epsilon_0 + \sigma_{\text{ave}}\Delta t} E_z|_1^n \\ &+ \frac{2\Delta t}{\Delta x\,(2\epsilon_{r,\infty,\text{ave}}\epsilon_0 + \sigma_{\text{ave}}\Delta t)} \\ &\cdot \left(H_y|_{3/2}^{n+1/2} - H_y|_{1/2}^{n+1/2} \right) \\ &- \frac{2\alpha\Delta t}{2\epsilon_{r,\infty,\text{ave}}\epsilon_0 + \sigma_{\text{ave}}\Delta t} \sum_{k=1}^{P} J_{z,k}|_1^n \end{aligned} \tag{15}$$

where the magnetic field $H_y|_{1/2}$ in updated as described above. In (15), we use (12) and (14) for the averaged permittivity and conductivity. The variables $J_{z,k}$ and $P_{z,k}$ are updated completely analogously to $K_{z,k}$ and $M_{z,k}$ in (10).

III. Validation of the Proposed Model

A. Pulse Reflection From a Coated Ideal Conductor

We start with a problem of a TE-polarized pulse reflecting from a metal wall coated with a dispersive layer. We consider a fixed set of material parameters of the coating, and calculate the numerical reflection coefficients and time-domain waveforms varying the thickness of the coating. The numerical results are then compared to the exact results.

1) Frequency-Domain Validation: Consider as an example a layer of a material whose relative permittivity and permeability are shown in Fig. 2. The parameters are of the Lorentz type. The permittivity has one resonance, while the permeability has two resonances. The parameters for the permeability are $\mu_\infty = 1$, $\beta_{m,1} = 4\cdot 10^{20}$ (rad/s)^2, $\beta_{m,2} = 1.25\cdot 10^{21}$ (rad/s)^2, $\omega_{pm,1} = 2\cdot 10^{10}$ (rad/s), $\omega_{pm,2} = 5\cdot 10^{10}$ (rad/s), $\gamma_{m,1} = \gamma_{m,2} = 1$, $\delta_{m,1} = 5\cdot 10^9$ rad/s, and $\delta_{m,2} = 4\cdot 10^9$ rad/s. The permittivity has parameters $\epsilon_\infty = 2$, $\beta_{e,1} = 9\cdot 10^{20}$ (rad/s)^2, $\omega_{pe,1} = 3\cdot 10^{10}$ rad/s, $\gamma_{e,1} = 1$, and $\delta_{e,1} = 5\cdot 10^8$ rad/s. The electrical conductivity is taken to be zero. The goal here is to demonstrate how the thickness of the coating affects the results. Hence, the above parameters are kept fixed and the thickness of the layer is varied in the numerical examples below.

The fields are recorded one cell away from the PEC boundary. Notice that a confident comparison of the phase of the reflection coefficient is only possible provided that the thickness of the layer is close to Δx since the electric field on the air–coating interface is not available unless $d = \Delta x$. For the magnitude of the reflection coefficient, this is not critical in this 1-D case. Only the magnitude of the reflection coefficient is shown for thinner coatings.

The magnitude and phase of the reflection coefficient in the case when $d = 0.9\Delta x = 1.8$ mm are shown in Fig. 3. Rather good agreement with the exact results is obtained. In Fig. 3(a), the largest discrepancy occurs near the second resonance, corresponding to the pole of the permittivity. The jump discontinuity of the phase of the reflection coefficient in Fig. 3(b) occurs at slightly smaller frequency than it should. Anyway, every resonance of the layer is qualitative very well and quantitatively rather accurately modeled.

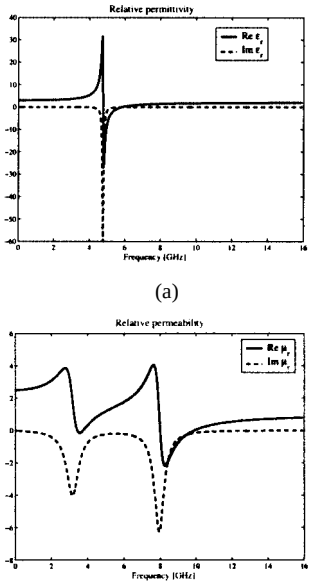

Fig. 2. (a) Relative permittivity of the coating. (b) Relative permeability of the coating.

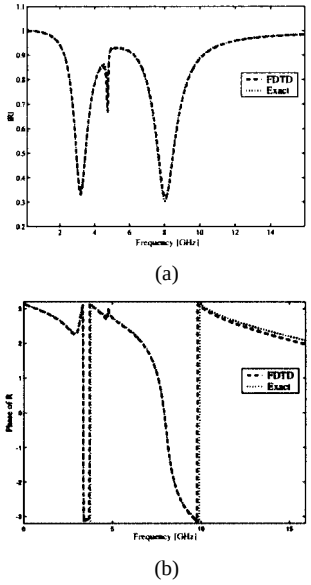

Fig. 3. (a) Magnitude of the reflection coefficient. (b) Phase of the reflection coefficient. The material parameters as a function of frequency are shown in Fig. 2.

Next, we decrease the thickness of the coating, choosing $d = 0.5\Delta x = 1$ mm. The numerically calculated and exact magnitude of the reflection coefficient as a function of frequency are shown in Fig. 4(a). It is observed that the resonance associated with the permittivity is not so strong, as in Fig. 3(a). In Fig. 4(a), there is almost zero reflection at approximately 8 GHz, the position of the second resonance of the permeability. Further decreasing the thickness of the coating, we set $d = 0.1\Delta x = 0.2$ mm. The result is presented in Fig. 4(b). The resonance associated to the permittivity near 4.8 GHz has almost been smeared out, and the dips are not so deep, as in the case of a thicker coating. These results show that the model works properly when the thickness of the coating is varied and also verifies that the

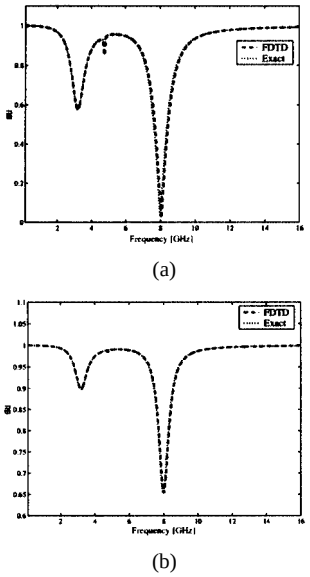

Fig. 4. (a) Magnitude of the reflection coefficient. Layer thickness $d = 1$ mm. (b) Magnitude of the reflection coefficient. Layer thickness $d = 0.2$ mm.

magnetic properties of the coating dominate when the coating is electrically very thin. Simulations for smaller damping factors for permeability were made, and very good agreement was observed even in that case. However, a more realistic case, where the maximum real part of the permeability in the considered frequency range is approximately four, was chosen as a numerical example.

2) Time-Domain Validation: We show some time-domain waveforms for the cases considered above. The incident electric field is a differentiated Gaussian pulse throughout the simulations. The exact reflected electric field on the interface as a function of time may be calculated via inverse Fourier transform. Thus, the integral

$$E_z^{\text{ref}}(t) = \frac{1}{\sqrt{2\pi}} \int_{-\infty}^{\infty} R(\omega) E_z^{\text{inc}}(\omega) e^{j\omega t}\, d\omega \qquad (16)$$

must be evaluated. The total field is obtained by replacing $R(\omega)$ with $1 + R(\omega)$ in the expression above. The surface impedance model may be used to calculate the exact reflection coefficient. In this problem, the PEC-backed coating can be modeled with a surface impedance of the form

$$Z_s(\omega) = j\sqrt{\frac{\mu(\omega)}{\epsilon(\omega)}} \tan\left(\sqrt{\epsilon(\omega)\mu(\omega)}\omega d\right) \qquad (17)$$

The exact reflection coefficient as a function of frequency is then obtained from

$$R = \frac{Z_s(\omega) - \eta_0}{Z_s(\omega) + \eta_0} \qquad (18)$$

where η_0 is the free-space wave impedance. The material parameters in Fig. 2 were used to calculate the results in Figs. 5 and 6. The agreement with the exact results is seen to also be good in the time domain. It is seen that the oscillations of the reflected wave become smaller when the thickness of the coating is decreased. This is natural since a PEC wall is obtained in the limit $d = 0$.

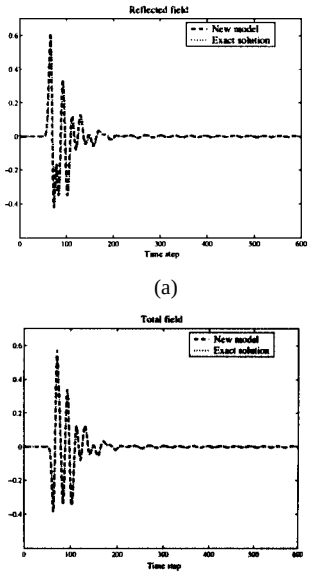

Fig. 5. (a) Reflected waveform on the boundary. $d = 1.8$ mm. (b) Total waveform on the boundary. $d = 1.8$ mm.

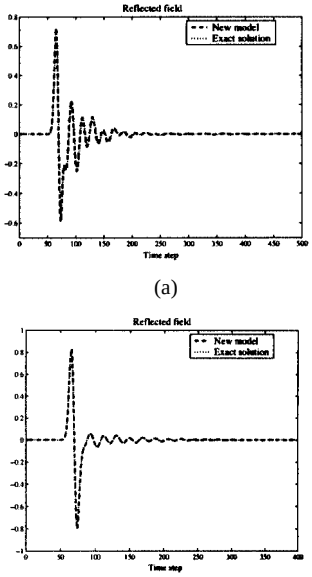

Fig. 6. (a) Reflected waveform on the boundary. $d = 1$ mm. (b) Reflected waveform on the boundary. $d = 0.2$ mm.

B. Cutoff Frequency of a Loaded Waveguide

First, consider a rectangular waveguide with the widths of the walls equal to $a = 30$ mm and $b = 15$ mm. Suppose there is a thin magnetic layer of thickness d along the broader wall in the middle of the waveguide. The permeability of the layer is taken to be of the Lorentz type with a single pole pair. In the lossless case, we may calculate the exact cutoff frequencies of this waveguide. Contrary to the previous example, we keep the thickness of the layer fixed and present a more detailed validation of the model by varying the material parameters and by comparing with the exact results. For a single pole-pair lossless Lorentz layer, there are three parameters to vary, i.e., μ_∞, $\beta_m = \omega_{pm}^2$, and ω_{0m}.

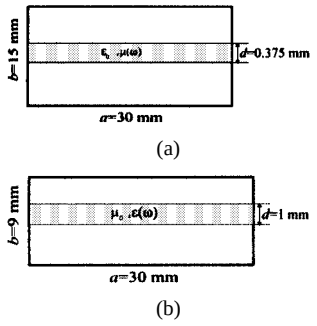

Fig. 7. (a) Cross section of a rectangular waveguide with perfectly conducting walls loaded with a dispersive magnetic layer of the Lorentz type. (b) Cross section of a rectangular waveguide loaded with a dispersive dielectric layer of the Lorentz type. The thickness of the layer is exaggerated here.

The problem geometries are shown in Fig. 7. Before numerical examples, we present an analytical expression for the cutoff frequencies of the waveguide loaded with a dispersive layer. For the fundamental TE_{10} mode to be considered here, the field distributions over the small height of the waveguide remain almost uniform for the components tangential to the layer. Hence, the approximate expression for the propagation constant (the cross section of the waveguide is uniform in the x-direction) is applicable [12] as follows:

$$k_x = \sqrt{\omega^2 \frac{d\mu(\omega) + (b-d)\mu_0}{\dfrac{d}{\epsilon(\omega)} + \dfrac{b-d}{\epsilon_0}} - \left(\frac{\pi}{a}\right)^2}. \tag{19}$$

The cutoff frequency of the TE_{10} mode is obtained by requiring that $k_x = 0$ and solving for ω. Notice that the approximate analytical result does not see the position of the layer. However, (19) is very accurate for the TE_{10} mode, and reduces to the exact result for an empty waveguide if $\epsilon(\omega) = \epsilon_0$ and $\mu(\omega) = \mu_0$. Rigorous derivation of the exact cutoff frequency is omitted here because it would lead to extremely long and tedious transcendental equations without significant increase of accuracy for the TE_{10} mode. The cutoff frequency may be calculated in a 2-D FDTD program using, for instance, a differentiated Gaussian pulse point excitation inside the waveguide, and recording the time-domain waveforms at an observation point. The observed fields are transformed into the frequency domain and the peaks in the spectrum correspond to the cutoff frequencies of the different modes propagating in the waveguide.

The thickness of the layer is equal to $d = 0.25\Delta x = 0.25\Delta y = 0.375$ mm. Hence, we have discretized the cross section of the waveguide with a grid of 20×10 FDTD cells. We first take the permeability to be independent of the frequency and vary the relative permeability. As expected, the cutoff frequency of the TE_{10} mode is seen to decrease with increasing permeability. The agreement with the analytical results is rather good: the maximum relative error in Fig. 8(a) is approximately 1%.

The results for varying $\beta_m = \omega_{pm}^2$ are shown in Fig. 8(b). Here, we fix $\mu_\infty = 1$ and the resonant frequency of the layer is chosen to be less than the cutoff frequency of the TE_{10} mode of an empty waveguide. We have chosen $\omega_{0m} = 2 \cdot 10^{10}$ rad/s. The maximum relative error is less than 1%. In Fig. 9(a), $\omega_{0m} = 4{\cdot}10^{10}$ rad/s, being larger than the cutoff of an empty waveguide

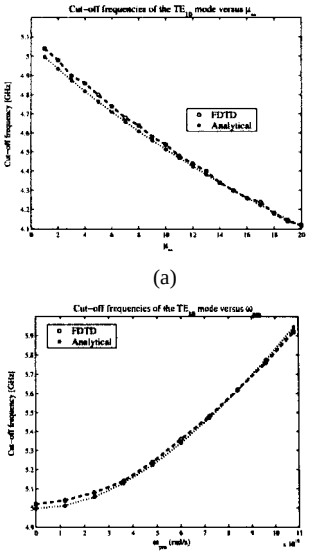

(a)

(b)

Fig. 8. (a) Numerical and analytical cutoff frequencies of the TE_{10} mode in the loaded waveguide versus μ_∞. (b) Numerical and analytical cutoff frequencies of the TE_{10} mode in the loaded waveguide versus ω_{pm}. The resonant frequency of the layer is smaller than the cutoff frequency of the TE_{10} mode of an empty waveguide.

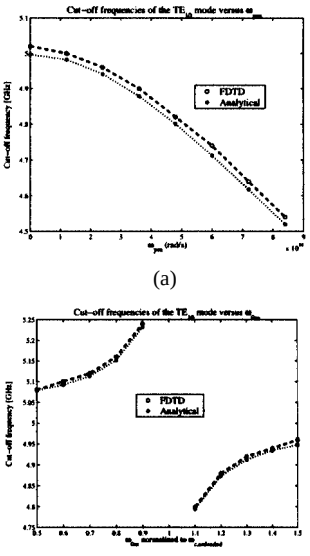

(a)

(b)

Fig. 9. (a) Numerical and analytical cutoff frequencies of the TE_{10} mode in the loaded waveguide versus ω_{pm}. The resonant frequency of the layer is larger than the cutoff frequency of the TE_{10} mode of an empty waveguide. (b) Numerical and analytical cutoff frequencies of the TE_{10} mode in the loaded waveguide versus ω_{0m}.

($\omega_{c,\mathrm{TE}_{10}} = \pi \cdot 10^{10}$ rad/s). The result is seen to be clearly different from that in Fig. 8(b).

In Fig. 9(b), we vary the resonant frequency of the layer around the cutoff frequency of the unloaded waveguide. We set $\mu_\infty = 1$ and $\omega_{pm} = \pi \cdot 10^{10}$ rad/s. The cutoff frequency of the loaded waveguide is seen to converge toward the cutoff frequency of the empty waveguide when we move away from the resonant frequency of the layer. More precisely, the cutoff frequency $f_{c,l}$ of the loaded waveguide tends to the cutoff frequency $f_{c,u}$ of the unloaded waveguide with increasing resonant frequency of the layer. On the other hand, $f_{c,l}$ remains

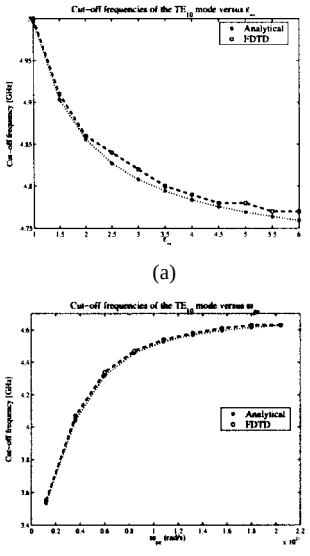

(a)

(b)

Fig. 10. (a) Numerical and analytical cutoff frequencies of the TE_{10} mode in the loaded waveguide versus ϵ_∞. (b) Numerical and analytical cutoff frequencies of the TE_{10} mode in the loaded waveguide versus ω_{pe}. The resonant frequency of the layer is smaller than the cutoff frequency of the TE_{10} mode in an empty waveguide.

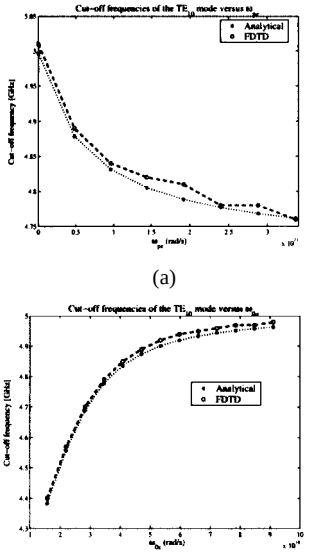

(a)

(b)

Fig. 11. (a) Numerical and analytical cutoff frequencies of the TE_{10} mode in the loaded waveguide versus ω_{pe}. The resonant frequency of the layer is larger than the cutoff frequency of the TE_{10} mode of an empty waveguide. (b) Numerical and analytical cutoff frequencies of the TE_{10} mode the loaded waveguide versus ω_{0e}.

slightly above $f_{c,u}$ even if the resonant frequency of the layer is arbitrarily small.

As regards the tangential components of the fields, the results presented thus far confirm that the proposed new model correctly works. We present one more example, where the normal components are also affected. We place a layer with a Lorentzian permittivity (with a single-pole pair) in the middle of the waveguide and calculate the cutoff frequencies versus the parameters of the layer. The shorter wall of the waveguide is now supposed to be 9 mm, and the thickness of the layer is equal to

1 mm. The layer thickness is increased from the previous example to observe a significant change in the cutoff frequency. It is seen from the analytical expression that the cutoff frequency is more sensitive to magnetic layers than to dielectric layers. The FDTD and analytical results are shown in Figs. 10 and 11. In Fig. 10(a), $\omega_{pe} = 0$, and ϵ_∞ is varied. In Fig. 10(b), $\epsilon_\infty = 1$, $\omega_{0e} = 2 \cdot 10^{10}$ rad/s and ω_{pe} is changed. This is also the case with the results in Fig. 11(a), except that $\omega_{0e} = 4 \cdot 10^{10}$ rad/s. Finally, in Fig. 11(b), $\epsilon_\infty = 1$, $\omega_{pe} = \pi \cdot 10^{10}$ rad/s, and the resonant frequency ω_{0e} of the layer is varied. The maximum relative error of the cutoff frequency is at most 1% in all the cases considered in this paper.

IV. Conclusions

A new model for treating electrically thin dispersive layers and coatings in FDTD simulations was introduced. The model is based on an appropriate averaging of the electric and magnetic flux densities and on the use of auxiliary quantities like polarization current and magnetization. The most important feature of the model is its ability to accurately model dispersive layers having multiple resonances of material parameters. The model is applicable for electrically thin layers. A great advantage of the model is that we do not have to consider the angle of incidence of the incident waves because the local nature of the model accounts for oblique incidence as well. With the proposed model, the use of cumbersome SIBCs for dispersive layers having multiple pole pairs is avoided. The proposed model was numerically verified with a couple of test problems by comparison with the analytical results. The results given both in time and frequency domains indicate rather good accuracy of the model. The model was found to be suitable for the analysis of waveguides loaded with a dispersive layer.

References

[1] C. F. Lee, R. T. Shin, and J. A. Kong, "Time domain modeling of impedance boundary conditions," *IEEE Trans. Microwave Theory Tech.*, vol. 40, pp. 1847–1850, Sept. 1992.

[2] B. Z. Wang, "Time-domain modeling of the impedance boundary condition for an oblique incident parallel-polarization plane wave," *Microwave Opt. Technol. Lett.*, vol. 7, pp. 19–22, 1994.

[3] ——, "Time-domain modeling of the impedance boundary condition for an oblique incident perpendicular-polarization plane wave," *Microwave Opt. Technol. Lett.*, vol. 7, pp. 355–359, 1994.

[4] C. W. Penney, R. J. Luebbers, and J. W. Schuster, "Scattering from coated targets using a frequency-dependent, surface impedance boundary condition in FDTD," *IEEE Trans. Antennas Propagat.*, vol. 44, pp. 434–443, Apr. 1996.

[5] P. A. Tirkas and K. R. Demarest, "Modeling of thin dielectric structures using the finite-difference time-domain method," *IEEE Trans. Antennas Propagat.*, vol. 39, pp. 1338–1344, Sept. 1991.

[6] J. G. Maloney and G. S. Smith, "The efficient modeling of thin material sheets in the finite-difference time-domain (FDTD) method," *IEEE Trans. Antennas Propagat.*, vol. 40, pp. 323–330, Mar. 1992.

[7] R. J. Luebbers and K. Kunz, "FDTD modeling of thin impedance sheets," *IEEE Trans. Antennas Propagat.*, vol. 40, pp. 349–351, Mar. 1992.

[8] C. J. Railton and J. P. McGeehan, "An analysis of microstrip with rectangular and trapezoidal conductor cross sections," *IEEE Trans. Antennas Propagat.*, vol. 38, pp. 1017–1022, Aug. 1990.

[9] L.-K. Wu and L.-T. Han, "Implementation and application of resistive sheet boundary condition in the finite-difference time-domain method," *IEEE Trans. Antennas Propagat.*, vol. 40, pp. 628–633, June 1992.

[10] J. G. Maloney and G. S. Smith, "A comparison of methods for modeling electrically thin dielectric and conducting sheets in the finite-difference time-domain method," *IEEE Trans. Antennas Propagat.*, vol. 41, pp. 690–694, May 1993.

[11] J. L. Young, "Propagation in linear dispersive media: Finite-difference time-domain methodologies," *IEEE Trans. Antennas Propagat.*, vol. 43, pp. 422–426, Apr. 1995.

[12] S. A. Tretyakov, A. S. Cherepanov, and M. I. Oksanen, "Averaging method for analysing waveguides with anisotropic filling," *Radio Sci.*, vol. 26, no. 2, pp. 523–528, 1991.

Mikko K. Kärkkäinen was born in Iisalmi, Finland, on July 22, 1976. He received the Master of Science degree in mathematics from the Helsinki University of Technology, Helsinki, Finland, in 2000, and is currently working toward the doctoral degree at the Helsinki University of Technology.

He is currently with the Radio Laboratory, Helsinki University of Technology. His main scientific interest is the development of new numerical models using the FDTD method.

Mr. Kärkkäinen is a member of the Finnish Graduate School of Electronics, Telecommunications, and Automation (GETA).